First Measurements of Electrons and Waves inside an Electrostatic Solitary Wave

H. S. Fu,[1,*] F. Chen,[1] Z. Z. Chen,[1] Y. Xu,[1] Z. Wang,[1] Y. Y. Liu,[1] C. M. Liu,[1] Y. V. Khotyaintsev,[2] R. E. Ergun,[3] B. L. Giles,[4] and J. L. Burch[5]

[1]*School of Space and Environment, Beihang University, Beijing 100191, China*
[2]*Swedish Institute of Space Physics, Uppsala 75121, Sweden*
[3]*Department of Astrophysical and Planetary Sciences, University of Colorado Boulder, Boulder, Colorado 80303, USA*
[4]*NASA Goddard Space Flight Center, Greenbelt, Maryland 20771, USA*
[5]*Southwest Research Institute, San Antonio, Texas 78228, USA*

(Received 3 September 2019; revised manuscript received 8 November 2019; accepted 14 February 2020; published 3 March 2020)

Electrostatic solitary wave (ESW)—a Debye-scale structure in space plasmas—was believed to accelerate electrons. However, such a belief is still unverified in spacecraft observations, because the ESW usually moves fast in spacecraft frame and its interior has never been directly explored. Here, we report the first measurements of an ESW's interior, by the Magnetospheric Multiscale mission located in a magnetotail reconnection jet. We find that this ESW has a parallel scale of $5\lambda_{De}$ (Debye length), a superslow speed (99 km/s) in spacecraft frame, a longtime duration (250 ms), and a potential drop $e\varphi_0/kT_e \sim 5\%$. Inside the ESW, surprisingly, there is no electron acceleration, no clear change of electron distribution functions, but there exist strong electrostatic electron cyclotron waves. Our observations challenge the conventional belief that ESWs are efficient at particle acceleration.

DOI: 10.1103/PhysRevLett.124.095101

The electrostatic solitary wave (ESW), sometimes referred to as electron phase space hole, is characterized by a bipolar variation of parallel electric fields associated with the potential drop [1–4] and is known as a consequence of electron depletion. Such a structure is typically generated by field-aligned streaming instabilities, such as the Buneman instability [5–9] and two-stream instability [3,10,11]. It exists ubiquitously in space plasmas, including the plasma sheet [7,8,12–15], auroral region [14,16–19], magnetopause [20,21], magnetosheath [22], bow shock [23,24], reconnection sites [7,25], and the solar wind [26]; also, it can exist in laboratory plasmas [27–29].

Although the ESW has been widely studied, previous spacecraft observations primarily focused on its scale and its interaction with ambient electrons. For example, Franz *et al.* [30] found that the ESW has a scale on the order of Debye length; Steinvall *et al.* [31] computed the perpendicular scale of the ESW by using multispacecraft data; Mozer *et al.* [32] presented the electron spectra and pitch angle distributions on a millisecond timescale around the ESW. Khotyaintsev *et al.* [7], Mozer *et al.* [33], and Vasko *et al.* [34] suggested electron acceleration around the ESW. These observations have made a substantial step forward in understanding the dynamics of ESWs. However, they are not sufficient, because electron distribution functions and waves inside the ESW have never been observed directly, due to the low resolution of spacecraft measurements (usually 4 s for particle data) and short-time duration of the ESW (usually several milliseconds) in previous studies. As a result, so far, there have been only computer simulations [27,35–37] and laboratory experiments [28,38] investigating the particle and wave dynamics inside the ESW.

To completely understand the dynamics of the ESW, revealing the electron distribution functions and waves by spacecraft measurements inside the ESW is necessary. To do so, the motion speed of the ESW must be slow in the spacecraft frame—to make sure that the spacecraft stay long enough inside the ESW, and also, the particle measurements must have high resolution—to make sure that the spacecraft collect enough data points inside the ESW. Being aware of these two issues, we aim to report the first measurements of electron distribution functions and waves inside the ESW in this Letter. We use data from the Magnetospheric Multiscale (MMS) mission [39], because this mission provides particle data with a resolution up to 30 ms (electrons) or 150 ms (ions), readily meeting our requirements. Specifically, the instruments used are the Fast Plasma Investigation [40], the Flux Gate Magnetometer [41], the Search Coil Magnetometer [42], the Electric Double Probe (EDP) [43], and the Axial Double Probe [44].

Fortunately, we find a superslow ESW in the Earth's magnetotail. This structure was detected by MMS on 17 July 2017 at about 07:53:05 UT, when the four MMS spacecraft were located at [−18.14 −7.30 0.64] R_E in GSM coordinates [Figs. 1(a) and 1(b)], with interspacecraft separations of 20 km [Figs. 2(a) and 2(b)]. Figures 1(c)–1(i) present an overview of the event, with the magnetic field shown in panel (c), electron density in panel (d), ion velocity shown in panel (e), electron temperature shown in panel (f),

electron flux in panel (g), ion flux in panel (h), and the parallel electric field shown in panel (i). Before 07:52:52 UT, MMS observed a weak magnetic field [$|B| < 3$ nT, Fig. 1(c)], a high plasma density [Ne > 0.2 cm^{-3}, Fig. 1(d)], and a large plasma β (not shown), meaning that it was located in the magnetotail plasma sheet [45]. Around 07:52:56 UT, MMS detected a sudden increase of magnetic field from Bz ≈ 2 nT to Bz ≈ 10 nT [Fig. 1(c)], a significant drop of plasma density from Ne ≈ 0.25 cm^{-3} to Ne ≈ 0.13 cm^{-3} [Fig. 1(d)], a slight increase of electron temperature from Te ≈ 2 keV to Te ≈ 2.5 keV [Fig. 1(f)], and a gradual increase of ion flow speed from Vi ≈ 400 km/s to Vi ≈ 800 km/s [Fig. 1(e)]. Such an abrupt change, from 07:52:55 to 07:52:59 UT, can be identified as a dipolarization front (DF) [46–52]. The duration of such DF (4 s) is consistent with previous statistics [53]. Behind the DF, from 07:53:00 to 07:53:15 UT, MMS detected a strong magnetic field [$|B| \approx 15$ nT, see Fig. 1(c)], low plasma density [Ne < 0.12 cm^{-3}, see Fig. 1(d)], large flow

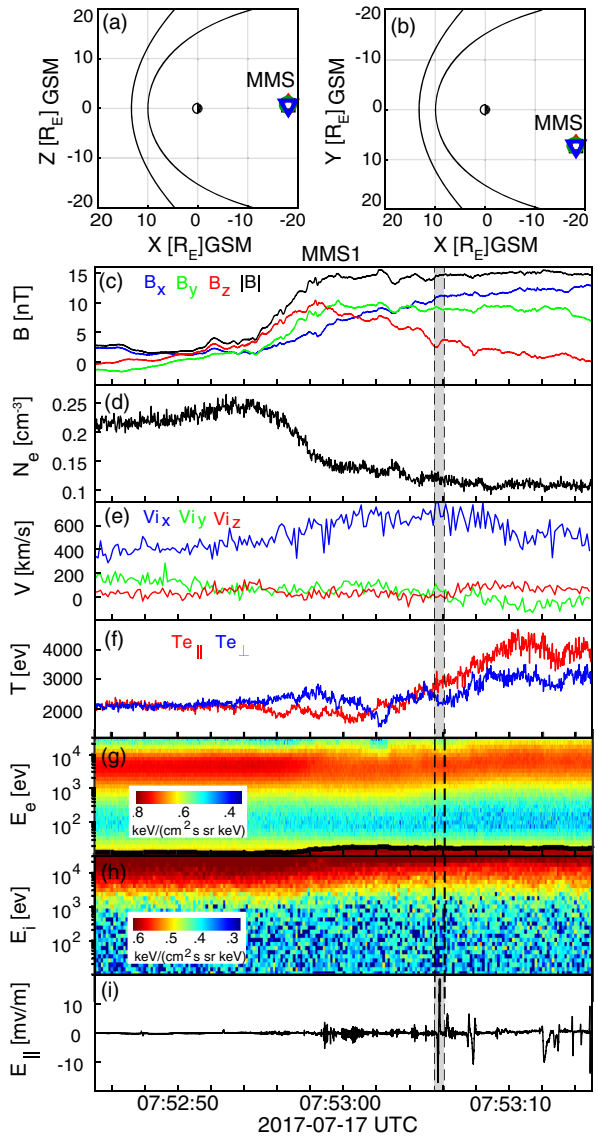

FIG. 1. An ESW observed by MMS1 on 17 July 2017. (a), (b) The MMS locations in X-Z and X-Y planes in GSM coordinates. (c) Magnetic field. (d) Plasma density. (e) Ion bulk flow velocities. (f) The electron temperature in parallel and perpendicular directions. (g) The differential energy fluxes of electrons. (h) The differential energy fluxes of ions. (i) Parallel electric field. The gray shade between the two black dotted lines highlights the ESW structure.

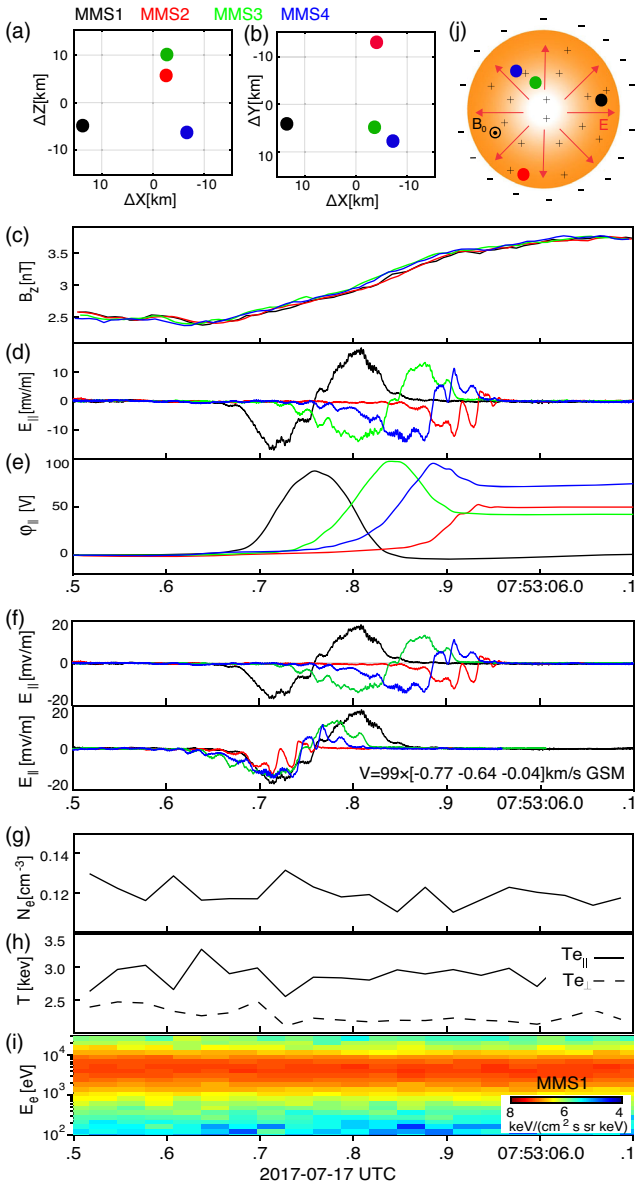

FIG. 2. Properties of the ESW. (a),(b) The MMS configuration in (a) the X-Z and (b) X-Y planes in GSM coordinates. (c) The magnetic field Bz components. (d) Parallel electric field. (e) Electrostatic potential. (f) The multispacecraft timing analysis of the ESW speed. (g)–(i) The MMS1 measurements of electron density, electron temperature, and omnidirectional electron fluxes. (j) A schematic of the ESW in the X-Y plane, with the red arrows denoting the electric fields and the plus and minus signs representing the charge.

velocity [Vi ≈ 800 km/s, see Fig. 1(e)], and high electron temperature [Te ≈ 3.5 keV, see Fig. 1(f)]. Such ion flow associated with a strong magnetic field can be identified as a reconnection jet [54–56] or dipolarizing flux buddle (DFB) [57].

Inside the reconnection jet, MMS observed a bipolar variation of parallel electric fields, from −18 mV/m to +18 mV/m, near the flow-velocity peak at 07:53:05.8 UT [see the vertical shade in Fig. 1(i)]. Since the magnetic field at that time (07:53:05.8 UT) is primarily in X_{GSM} and Y_{GSM} directions [see the vertical shade in Fig. 1(c)], this electric field should be primarily along the X_{GSM} and Y_{GSM} directions, and thus it was measured primarily by the EDP instrument [43]. We examine the raw data in the spacecraft-fixed coordinates (not shown) and find that both the EDP and Axial Double Probe [44] instruments captured this bipolar variation of $E_{\parallel}$, indicating that the bipolar variation in this event is real, but not instrumental noise. Moreover, all of the four MMS spacecraft detected this signature, making us very confident that the bipolar variation is a real structure.

Figure 2 presents the details of this structure during 07:53:05.667–07:53:05.967 UT. As can be seen, the structure was sequentially detected by MMS1, MMS3, MMS4, and MMS2 [Fig. 2(d)]. It produces an electrostatic potential, $\varphi = -\int E_{\parallel} v_{eh} dt$, up to 100 V [Fig. 2(e)], and thus it is an ESW structure. We use the multispacecraft timing method [Fig. 2(f)] to estimate the drift speed of this ESW as $V_{ESW} \approx 99^{*}[-0.77 - 0.64 - 0.04]$ km/s (GSM coordinates) in the spacecraft frame. Such speed is superslow, compared with the local Alfven velocity ($V_A \approx 953$ km/s) and electron thermal velocity ($V_{te} \approx 20\,000$ km/s). However, when transferred to the plasma-rest frame (Vi ≈ 800 km/s), this speed changes to $V_{te} \approx 20\,000$ km/s, which is comparable to the local Alfvén velocity and larger than the drift speeds reported in previous studies [8,58]. We estimate the parallel scale of this ESW as $L_{\parallel} = 0.5 t\, V_{ESW} \approx 5$ km $\approx 5\lambda_{De}$ ($\lambda_{De} \approx 1$ km is the Debye length), where $t \approx 100$ ms is the time duration between the minimum and maximum parallel electric fields [see Fig. 2(d)]. Such parallel scale ($5\lambda_{De}$) is consistent with previous statistics [30], where a parallel scale $<10\lambda_{De}$ was suggested for most ESWs. Since the ESW was sequentially detected by four MMS spacecraft, it should have perpendicular scale ($L_{\perp}$) larger than 20 km, the interspacecraft separation of MMS. We can estimate the perpendicular scale by using the gyrokinetic scaling relation [59], $L_{\perp}/L_{\parallel} \sim (1+\omega_{pe}^2/\omega_{ce}^2)^{1/2} \sim 7$, where $\omega_{pe} \approx 1.96 \times 10^4$ rad/s is the plasma frequency and $\omega_{ce} \approx 2.57 \times 10^3$ rad/s is the electron cyclotron frequency. In this way, we obtain the perpendicular

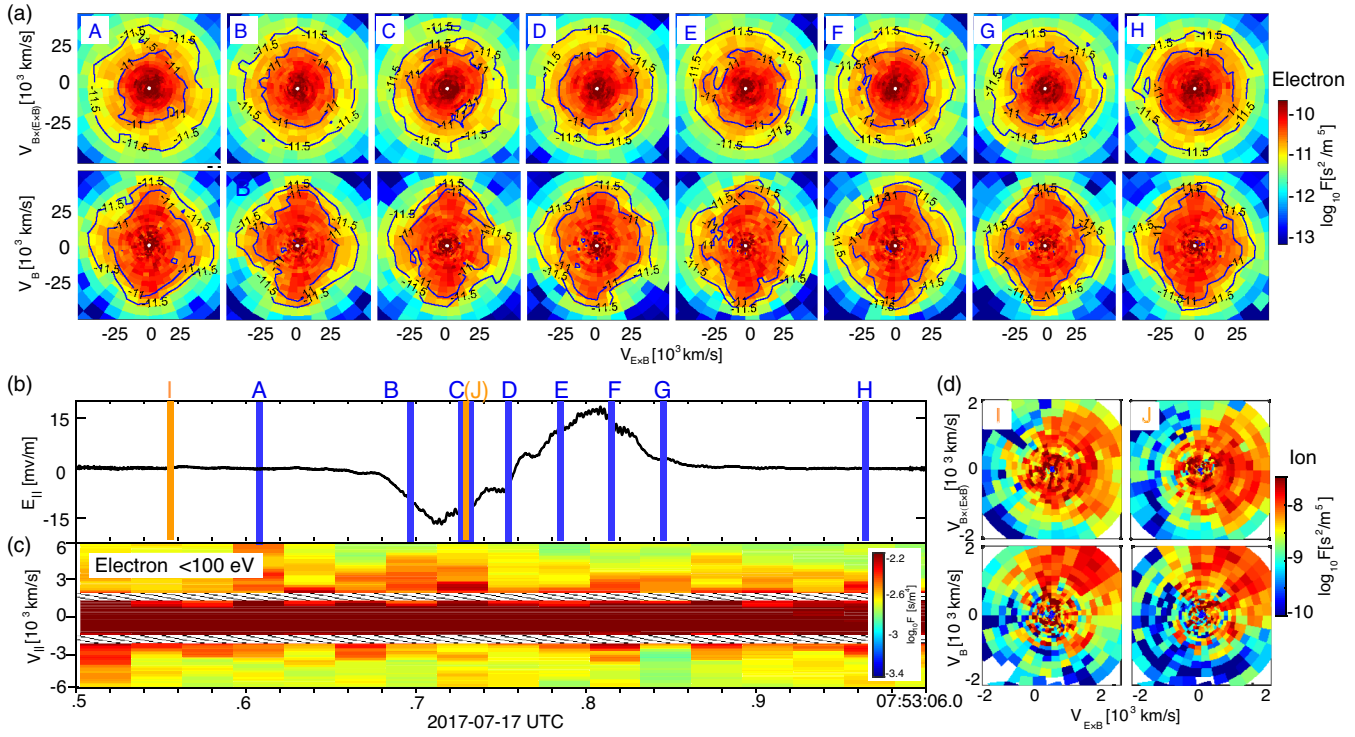

FIG. 3. Electron and ion distribution functions. (a) The electron distribution functions inside (B, C, D, E, F, G) and outside (A, H) the ESW, with the black lines denoting contours of the phase space density. At the center of each panel, the white spot indicates no data, because those electrons are beyond the measurement range (<6.52 eV) of the Fast Plasma Investigation instrument. (b) The parallel electric field. (c) The parallel phase space density of electrons. (d) The ion distribution functions inside (J) and outside (I) the ESW. Here, the perpendicular plane is defined as ($\mathbf{V_{E\times B}}$, $\mathbf{V_{B\times(E\times B)}}$), and the parallel plane is defined as ($\mathbf{V_{E\times B}}$, $\mathbf{V_B}$).

scale of the ESW as $35\lambda_{De}$. Figure 2(j) illustrates this ESW in the perpendicular plane, with its shape derived from the double-Gaussian potential model [8,60–64], $\varphi(z,r) = \varphi_0 e^{-z^2/2L_\parallel{}^2} e^{-r^2/2L_\parallel{}^2}$.

Since the drift speed of this ESW is superslow in the spacecraft frame, MMS1 stayed for about 250 ms inside the ESW [from 07:53:05.65 to 07:53:05.90 UT, see Fig. 2(d)]. This provides a very good opportunity to explore electron dynamics inside the ESW, particularly when considering that the data resolution of electron measurements is 30 ms. Figure 3(a) presents the electron distribution functions (measured by MMS1) inside and around this ESW, with the first row showing the distribution in the perpendicular plane ($V_{E\times B}$, $V_{B\times(E\times B)}$) and the second row showing the distribution in the parallel plane ($V_{E\times B}$, V_B). Specifically, two snapshots outside the ESW [A and H, see Fig. 3(b)] and six snapshots inside the ESW [B–G, see Fig. 3(b)] are considered. During the whole interval, MMS1 observed gyrotropic distribution in the perpendicular plane [Fig. 3(a), first row] and rolling-pin distribution [65,66] in the parallel plane [Fig. 3(a), second row]. Such gyrotropic distribution is expected, because during this interval the magnetic field has no reversal. The rolling-pin distribution, showing pitch angles primarily at 0°, 90°, and 180°, appears quite often behind the DF [65,66]. Interestingly, the electron distribution functions inside and outside the ESW are very similar (in both parallel and perpendicular planes) (see the quantitative comparison in Supplemental Material S1 [67]), meaning that the ESW had negligible effects on the distribution function, or in other words, it did not change the electron dynamics considerably. In fact, inside the ESW, the electron density [Fig. 2(g)], electron temperature [Fig. 2(h)], and omnidirectional electron fluxes [Fig. 2(i)] are all not changed, meaning that there is no electron acceleration and heating in this event. Such observation does not support previous studies [7,21,32,68], where strong electron acceleration was speculated inside the ESW.

Actually, if the acceleration occurs, it should change the parallel velocity of the trapped electrons (<100 eV), because the ESW in this event produces an electrostatic potential of 100 V in the parallel direction [see Fig. 2(e)]. However, we examine the parallel and antiparallel phase space density of the 10–100 eV electrons (2000–6000 km/s) and find no clear change inside the ESW [see Fig. 3(c)]. This strongly confirms that the electron acceleration and heating do not occur in this event. Notice that the zebra stripes in Fig. 3(c) indicate the spacecraft potential in this event (10 eV or equivalently 2000 km/s), below which photoelectron contaminations may exist and spacecraft measurements of electrons in such range (<2000 km/s) are not reliable.

We can also examine whether the ESW interacts with ions. Figure 3(d) presents the ion distribution functions inside and outside the ESW (measured by MMS1), in the same format as Fig. 3(a). As can be seen, the distribution functions inside (J) and outside (I) the ESW are quite similar [Fig. 3(d)], meaning that there is no significant interaction between ions and the ESW. This does not support previous studies [18], where strong ion heating was speculated.

We further investigate wave emissions inside the ESW. Figure 4 presents a wave spectrogram of the parallel electric field (b), perpendicular electric field (c), and magnetic field (d). As can be seen, inside the ESW, strong wave emissions are found in both the parallel and perpendicular electric fields from 300 to 700 Hz [Figs. 4(b) and 4(c)], but not found in the magnetic field [Fig. 4(d)]. We apply a bandpass filter to obtain the waveform data of the electric and magnetic field in the frequency range of 300–700 Hz (not shown), and then estimate the phase speed of the waves as $|\delta E'_\perp/\delta B'_\parallel| \approx 5\times10^6$ km/s. Such speed is much larger than the local Alfvén speed, meaning that these waves are electrostatic. Interestingly, in the parallel electric field [Fig. 4(b)] the wave appears in the outer part of the ESW, while in the perpendicular electric field [Fig. 4(c)] the wave appears in the central part of the ESW. Since the frequency of these waves is near the electron gyrofrequency (f_{ce}, red line), we can identify them as the electrostatic electron cyclotron waves [69]. Such waves theoretically

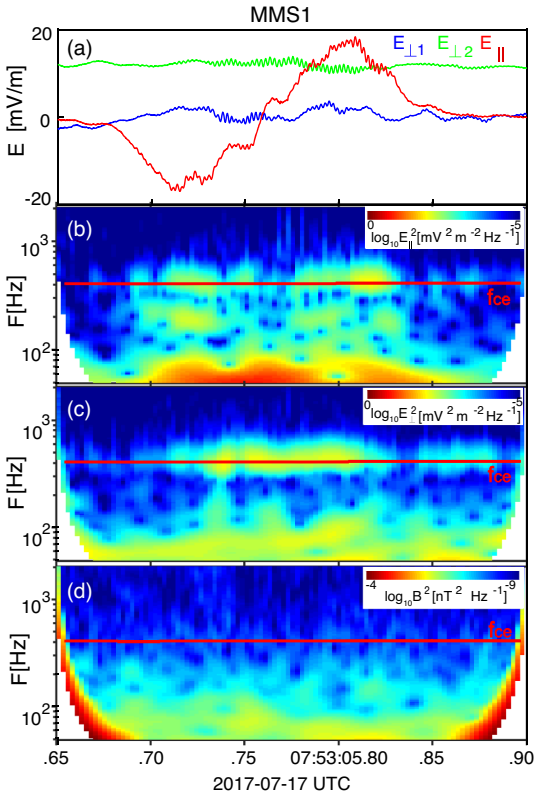

FIG. 4. The wave spectrum. (a) Perpendicular electric fields and parallel electric fields observed by MMS1. (b)–(d) The wave spectrum of the parallel electric field, perpendicular electric field, and magnetic field. The red solid line denotes the electron gyrofrequency.

can scatter electrons to change the distribution function [70,71]. However, in this event, the distribution function had no clear change [Fig. 3(a)], probably because wave-particle interactions are weak. In fact, we cannot find such waves at high harmonics of the electron gyrofrequency [Figs. 4(b) and 4(c)], suggesting that the wave-particle interactions are indeed weak.

In summary, we observe an ESW in the magnetotail reconnection jet, and investigate the electron distribution functions and wave emissions inside this ESW. We find strong electron cyclotron waves inside the ESW, but find no electron acceleration and heating there. Although there have been some previous studies [7,32] discussing the ESW's interior, directly showing distribution functions and wave emissions inside the ESW, to our knowledge, is the first time. The amplitude (18 mV/m) and motion speed (900 km/s in the plasma-rest frame) of ESW in this event are similar to those reported in previous studies [8,58], meaning that this event can be a good representative of ESWs in space and probably the new findings in this event can appear in other ESWs. Indeed, we find three other events on the same day (17 July 2017), showing no electron acceleration and electron heating inside the ESWs (see Supplemental Material S2 [67]), supporting our conclusions very well. In this sense, our observations may challenge the conventional belief that ESWs are efficient at particle acceleration.

We thank the MMS Data Center for providing the data. This work was supported by NSFC Grants No. 41821003 and No. 41874188.

*huishanf@gmail.com

[1] H. Schamel, Phys. Rep. **140**, 161 (1986).
[2] L. Muschietti, R. E. Ergun, I. Roth, and C. W. Carlson, Geophys. Res. Lett. **26**, 1093 (1999).
[3] I. H. Hutchinson, Phys. Plasmas **24**, 055601 (2017).
[4] H. Aravindakshan, A. Kakad, and B. Kakad, Phys. Plasmas **25**, 052901 (2018).
[5] C. Cattell *et al.*, J. Geophys. Res. **110**, A01211 (2005).
[6] H. Che, J. F. Drake, and M. Swisdak, and P. H. Yoon, Geophys. Res. Lett. **37**, L11105 (2010).
[7] Y. V. Khotyaintsev, A. Vaivads, M. André, M. Fujimoto, A. Retinò, and C. J. Owen, Phys. Rev. Lett. **105**, 165002 (2010).
[8] C. Norgren, M. Andre, and A. Vaivads, Geophys. Res. Lett. **42**, 1654 (2015).
[9] C. Norgren, M. André, D. B. Graham, Y. V. Khotyaintsev, and A. Vaivads, Geophys. Res. Lett. **42**, 7264 (2015).
[10] Y. Omura, H. Matsumoto, T. Miyake, and H. Kojima, J. Geophys. Res. **101**, 2685 (1996).
[11] D. L. Newman, M. Goldman, R. Ergun, and A. Mangeney, Phys. Rev. Lett. **87**, 255001 (2001).
[12] H. Matsumoto, H. Kojima, T. Miyatake, Y. Omura, M. Okada, I. Nagano, and M. Tsutsui, Geophys. Res. Lett. **21**, 2915 (1994).
[13] C. M. Liu, A. Vaivads, D. B. Graham, Y. V. Khotyaintsev, H. S. Fu, A. Johlander, M. André, and B. L. Giles, Geophys. Res. Lett. **46**, 12702 (2019).
[14] C. Cattell, J. Dombeck, J. R. Wygant, M. K. Hudson, F. S. Mozer, M. A. Temerin, W. K. Peterson, C. A. Kletzing, C. T. Russell, and R. F. Pfaff, Geophys. Res. Lett. **26**, 425 (1999).
[15] R. E. Ergun, K. A. Goodrich, J. E. Stawarz, L. Andersson, and V. Angelopoulos, J. Geophys. Res. **120**, 1832 (2015).
[16] S. V. Singh, G. S. Lakhina, R. Bharuthram, and S. R. Pillay, Phys. Plasmas **18**, 122306 (2011).
[17] R. E. Ergun *et al.*, Geophys. Res. Lett. **25**, 2041 (1998).
[18] R. E. Ergun, C. W. Carlson, L. Muschietti, I. Roth, and J. P. McFadden, Nonlinear Processes Geophys. **6**, 187 (1999).
[19] Q. M. Lu, D. Y. Wang, and S. Wang, J. Geophys. Res. **110**, A03223 (2005).
[20] H. Matsumoto, X. H. Deng, H. Kojima, and R. R. Anderson, Geophys. Res. Lett. **30**, 1326 (2003).
[21] D. B. Graham, Y. V. Khotyaintsev, A. Vaivads, and M. André, J. Geophys. Res. **121**, 3069 (2016).
[22] J. Pickett *et al.*, Adv. Space Res. **41**, 1666 (2008).
[23] S. D. Bale, P. J. Kellogg, D. E. Larsen, R. P. Lin, K. Goetz, and R. P. Lepping, Geophys. Res. Lett. **25**, 2929 (1998).
[24] I. Y. Vasko, F. S. Mozer, V. V. Krasnoselskikh, A. V. Artemyev, O. V. Agapitov, S. D. Bale, L. Avanov, R. Ergun, B. Giles, P.-A. Lindqvist, C. T. Russell, R. Strangeway, and R. Torbert, Geophys. Res. Lett. **45**, 5809 (2018).
[25] F. S. Mozer, O. A. Agapitov, A. Artemyev, J. L. Burch, R. E. Ergun, B. L. Giles, D. Mourenas, R. B. Torbert, T. D. Phan, and I. Vasko, Phys. Rev. Lett. **116**, 145101 (2016).
[26] D. M. Malaspina, D. L. Newman, L. B. Willson, K. Goetz, P. J. Kellogg, and K. Kerstin, J. Geophys. Res. **118**, 591 (2013).
[27] J. F. Drake *et al.*, Science **299**, 873 (2003).
[28] W. Fox, M. Porkolab, J. Egedal, N. Katz, and A. Le, Phys. Rev. Lett. **101**, 255003 (2008).
[29] B. Lefebvre, L.-J. Chen, W. Gekelman, P. Kintner, J. Pickett, P. Pribyl, S. Vincena, F. Chiang, and J. Judy, Phys. Rev. Lett. **105**, 115001 (2010).
[30] J. R. Franz, P. M. Kintner, J. S. Pickett, and L.-J. Chen, J. Geophys. Res. **110**, A09212 (2005).
[31] K. Steinvall, Y. V. Khotyaintsev, D. B. Graham, A. Vaivads, P.-A. Lindqvist, C. T. Russell, and J. L. Burch, Geophys. Res. Lett. **46**, 55 (2019).
[32] F. S. Mozer, O. V. Agapitov, B. Giles, and I. Vasko, Phys. Rev. Lett. **121**, 135102 (2018).
[33] F. S. Mozer, O. V. Agapitov, A. Artemyev, J. F. Drake, V. Krasnoselskikh, S. Lejosne, and I. Vasko, Geophys. Res. Lett. **42**, 3627 (2015).
[34] I. Y. Vasko, O. V. Agapitov, F. S. Mozer, A. V. Artemyev, J. F. Drake, and I. V. Kuzichev, J. Geophys. Res. **122**, 120 (2017).
[35] A. Kakad, B. Kakad, and Y. Omura, Phys. Plasmas **24**, 060704 (2017).
[36] B. Kakad, A. Kakad, and Y. Omura, Phys. Plasmas **24**, 102122 (2017).
[37] Q. M. Lu, B. Lembege, J. B. Tao, and S. Wang, J. Geophys. Res. **113**, A11219 (2008).
[38] I. Y. Vasko, O. V. Agapitov, F. S. Mozer, and A. V. Artemyev, J. Geophys. Res. **120**, 8616 (2015).

[39] J. Burch, T. Moore, R. Torbert, and B. Gile, Space Sci. Rev. **199**, 5 (2016).
[40] C. Pollock *et al.*, Space Sci. Rev. **199**, 331 (2016).
[41] C. Russell *et al.*, Space Sci. Rev. **199**, 189 (2016).
[42] O. Le Contel *et al.*, Space Sci. Rev. **199**, 257 (2016).
[43] P.-A. Lindqvist *et al.*, Space Sci. Rev. **199**, 137 (2016).
[44] R. E. Ergun *et al.*, Space Sci. Rev. **199**, 167 (2016).
[45] J. B. Cao *et al.*, J. Geophys. Res. **111**, A04206 (2006).
[46] R. Nakamura, W. Baumjohann, B. Klecker, Y. Bogdanova, A. Balogh, H. Rème, J. M. Bosqued, I. Dandouras, J. A. Sauvaud, K.-H. Glassmeier, L. Kistler, C. Mouikis, T. L. Zhang, H. Eichelberger, and A. Runov, Geophys. Res. Lett. **29**, 3-1 (2002).
[47] H. S. Fu, Y. V. Khotyaintsev, M. André, and A. Vaivads, Geophys. Res. Lett. **38**, L16104 (2011).
[48] H. S. Fu, Y. V. Khotyaintsev, A. Vaivads, M. Andre, and S. Y. Huang, Geophys. Res. Lett. **39**, L06105 (2012).
[49] H. S. Fu, Y. V. Khotyaintsev, A. Vaivads, A. Retinò, and M. André, Nat. Phys. **9**, 426 (2013).
[50] C. M. Liu, H. S. Fu, Y. Xu, Y. V. Khotyaintsev, J. L. Burch, R. E. Ergun, D. G. Gershman, and R. B. Torbert, Geophys. Res. Lett. **45**, 4628 (2018).
[51] C. M. Liu *et al.*, Geophys. Res. Lett. **45**, 556 (2018).
[52] H. Fu, E. E. Grigorenko, C. Gabrielse, C. Liu, S. Lu, K. J. Hwang, X. Zhou, Z. Wang, and F. Chen, Sci. China Earth Sci. **63**, 235 (2020).
[53] H. S. Fu, Y. V. Khotyaintsev, A. Vaivads, M. Andre, and S. Y. Huang, Geophys. Res. Lett. **39**, L10101 (2012).
[54] H. S. Fu, Y. V. Khotyaintsev, A. Vaivads, M. André, V. A. Sergeev, S. Y. Huang, E. A. Kronberg, and P. W. Daly, J. Geophys. Res. **117**, A12221 (2012).
[55] H. S. Fu, Y. Xu, A. Vaivads, and Y. V. Khotyaintsev, Astrophys. J. Lett. **870**, L22 (2019).
[56] H. S. Fu, A. Vaivads, Y. V. Khotyaintsev, M. André, J. B. Cao, V. Olshevsky, J. P. Eastwood, and A. Retinò, Geophys. Res. Lett. **44**, 37 (2017).
[57] J. Liu, V. Angelopoulos, A. Runov, and X.-Z. Zhou, J. Geophys. Res. **118**, 2000 (2013).
[58] D. B. Graham, Y. V. Khotyaintsev, A. Vaivads, and M. André, Geophys. Res. Lett. **42**, 215 (2015).
[59] J. R. Franz, P. M. Kintner, C. E. Seyler, J. S. Pickett, and J. D. Scudder, Geophys. Res. Lett. **27**, 169 (2000).
[60] L.-J. Chen, D. J. Thouless, and J.-M. Tang, Phys. Rev. E **69**, 055401(R) (2004).
[61] L. Andersson *et al.*, Phys. Rev. Lett. **102**, 225004 (2009).
[62] J. B. Tao *et al.*, J. Geophys. Res. **116**, A11213 (2011).
[63] J. C. Holmes, R. E. Ergun, D. L. Newman, N. Ahmadi, L. Andersson, O. Le Contel, R. B. Torbert, B. L. Giles, R. J. Strangeway, and J. L. Burch, J. Geophys. Res. **123**, 9963 (2018).
[64] Y. Tong, I. Vasko, F. S. Mozer, S. D. Bale, I. Roth, A. V. Artemyev, R. Ergun, B. Giles, P.-A. Lindqvist, C. T. Russell, R. Strangeway, R. B. Torbert, Geophys. Res. Lett. **11**, 513 (2018).
[65] C. M. Liu, H. S. Fu, Y. Xu, J. B. Cao, and W. L. Liu, Geophys. Res. Lett. **44**, 6492 (2017).
[66] M. J. Zhao, H. S. Fu, C. M. Liu, Z. Z. Chen, Y. Xu, B. L. Giles, and J. L. Burch, Geophys. Res. Lett. **46**, 2390 (2019).
[67] See Supplemental Material at http://link.aps.org/supplemental/10.1103/PhysRevLett.124.095101 for the quantitative comparison of electron distribution functions around ESW and three other events showing no electron acceleration inside ESW.
[68] I. Y. Vasko, O. V. Agapitov, F. S. Mozer, A. V. Artemyev, V. V. Krasnoselskikh, and J. W. Bonnell, J. Geophys. Res. **122**, 3163 (2017).
[69] H. S. Fu *et al.*, J. Geophys. Res. **119**, 9089 (2014).
[70] B. Ni, Y. Shprits, M. Hartinger, V. Angelopoulos, X. Gu, and D. Larson, J. Geophys. Res. **116**, A04218 (2011).
[71] B. Ni, J. Liang, R. M. Thorne, V. Angelopoulos, R. B. Horne, M. Kubyshkina, E. Spanswick, E. F. Donovan, and D. Lummerzheim, J. Geophys. Res. **117**, A01218 (2012).